Marginally-Stable Thermal Equilibria of Rayleigh-Bénard Convection

Sharrod Brown
Senator (D), Ohio

A novel iterative time-marching method is derived by introducing time-dependence in the background temperature profile of the classical Rayleigh-Bénard Boussinesq linear stability analysis. Eigenfunction amplitudes are obtained by requiring marginal-stability. Symmetric thermally-equilibrated states are then obtained and their intrinsic properties are analyzed. Such states are compared with statistically-steady 2-dimensional Rayleigh-Beńard convection simulations: marginally-stable thermally-equilibrated states have thinner boundary layers which scale like $\delta \sim Ra^{-1/3}$. 2-dimensional simulations run with thermally-equilibrated initial conditions turn out to be kinetically exaggerated, consequently requiring increased computational expense when compared to the conventional diffusive initial condition.

I. INTRODUCTION

The introduction leads the reader from a general subject area to a particular topic of inquiry. It establishes the scope, context, and significance of the research being conducted by summarizing current understanding and background information about the topic, stating the purpose of the work in the form of the research problem supported by a hypothesis or a set of questions, explaining briefly the methodological approach used to examine the research problem, highlighting the potential outcomes your study can reveal, and outlining the remaining structure and organization of the paper.

II. CONVENTIONAL BOUSSINESQ LINEAR STABILITY ANALYSIS

We begin with the non-dimensionalized Boussinesq approximation for Rayleigh-Bénard Convection. The domain is 2-dimensional rectangular and horizontally periodic with spatial dimensions x and z where $0 < x < 4$ and $-1/2 < z < 1/2$. The fluid of interest is constrained between two planar boundaries at $z = -1/2$ and $z = 1/2$ with fixed temperatures 1 and 0 respectively. At both boundaries we specify impenetrable, no-slip conditions, such that the velocity $\mathbf{u} = u\hat{x} + w\hat{z} = \mathbf{0}$ at $z = \pm 1/2$. The equations of motion are then given by

$$\nabla \cdot \mathbf{u} = 0 \tag{1}$$

$$\frac{\partial \mathbf{u}}{\partial t} + \mathbf{u} \cdot \nabla \mathbf{u} = -\nabla p + T\hat{z} + \sqrt{\frac{Pr}{Ra}}\nabla^2 \mathbf{u} \tag{2}$$

$$\frac{\partial T}{\partial t} + \mathbf{u} \cdot \nabla T = \frac{1}{\sqrt{RaPr}}\nabla^2 T \tag{3}$$

where p is pressure and T is temperature. For completeness, we specify a final boundary condition $p = p_0$ at $z = \pm 1/2$. Any system of this form can be characterized by its Rayleigh number Ra and Prandtl number Pr, where Ra is the timescale ratio of thermal diffusion to convection and Pr is the ratio of momentum diffusivity to thermal diffusivity. For convenience, we define

$$\mathcal{R} = \sqrt{\frac{Pr}{Ra}}, \qquad \mathcal{P} = \frac{1}{\sqrt{PrRa}} \tag{4}$$

To derive the linearized system, we posit that each field can be represented as the sum of a background profile (denoted by $\bar{\cdot}$) and a perturbation function (denoted by $\cdot'$). Suppose $\frac{\partial \bar{T}}{\partial z}\big|_{t=t_0}(z)$ is some given function which satisfies

$$\int_{-\frac{1}{2}}^{\frac{1}{2}} \frac{\partial \bar{T}}{\partial z}\Big|_{t=t_0} dz = -1 \tag{5}$$

then the background profiles are given by

$$\bar{\mathbf{u}} = \mathbf{0} \tag{6}$$

$$\bar{T}(z) = 1 + \int_{-\frac{1}{2}}^{z} \frac{\partial \bar{T}}{\partial \zeta}\Big|_{t=t_0}(\zeta) d\zeta \tag{7}$$

$$\bar{p}(z) = p_0 - \int_{-\frac{1}{2}}^{z} \bar{T}(\zeta) d\zeta \tag{8}$$

Accordingly, the fields are rewritten as

$$\mathbf{u}(x,z,t) = \mathbf{u}'(x,z,t) \tag{9}$$

$$= u'(x,z,t)\hat{x} + w'(x,z,t)\hat{z} \tag{10}$$

$$T(x,z,t) = \bar{T}(z) + T'(x,z,t) \tag{11}$$

$$p(x,z,t) = \bar{p}(z) + p'(x,z,t) \tag{12}$$

Upon substitution, we equate terms which scale linearly with the perturbations, yielding the linearized stability equations

$$\nabla \cdot \mathbf{u}' = 0 \tag{13}$$

$$\frac{\partial \mathbf{u}'}{\partial t} = -\nabla p' + T'\hat{z} + \mathcal{R}\nabla^2 \mathbf{u}' \tag{14}$$

$$\frac{\partial T'}{\partial t} + \frac{\partial \bar{T}}{\partial z} w' = \mathcal{P}\nabla^2 T' \tag{15}$$

with Dirichlet boundary conditions

$$T'|_{z=\pm\frac{1}{2}} = 0, \quad u'|_{z=\pm\frac{1}{2}} = 0, \quad p'|_{z=\pm\frac{1}{2}} = 0 \tag{16}$$

In 1916, Lord Rayleigh observed that (13) and (15) can be manipulated into a separable form with generalized solutions

$$w'(x,z,t) = W(z)\, e^{i(k_x x - st)} \tag{17}$$

$$u'(x,z,t) = U(z)\, e^{i(k_x x - st)} \tag{18}$$

$$T'(x,z,t) = \Theta(z)\, e^{i(k_x x - st)} \tag{19}$$

$$p'(x,z,t) = P(z)\, e^{i(k_x x - st)} \tag{20}$$

where $s = \sigma + i\omega$ and k_x is constricted by periodicity to the countably infinite set (spectrum) of wavenumbers

$$k_x \in \left\{ \frac{n\pi}{2} \,\middle|\, n \in \mathbb{N} \right\} \tag{21}$$

For each k_x, we can assess the stability of the perturbations by solving for the eigenvalue s, whose imaginary component ω plays the role of an exponential growth rate. Solution yields a finite set of eigenvalues, among which, that with the maximum value of ω is assumed to be dominant. Positive eigenvalues indicate that the system is unstable to small disturbances of wavenumber k_x, while negative eigenvalues indicate stability. A complete linear stability analysis requires that we solve over the full spectrum of wavenumbers. The prototypical case is used to demonstrate that the critical Rayleigh number $Ra_c = 1708$ when $\frac{\partial \bar{T}}{\partial z}\big|_{t=t_0} = -1$.

III. TEMPERATURE PROFILE EVOLUTION

For this investigation, we allow $\bar{T}$ to vary in z and t. Substituting (11) into (3) yields

$$\frac{\partial \bar{T}}{\partial t} + \mathbf{u}' \cdot \nabla T' + \frac{\partial T'}{\partial t} + \frac{\partial \bar{T}}{\partial z} w' = \mathcal{P}\nabla^2 T' + \mathcal{P}\nabla^2 \bar{T}. \tag{22}$$

Subtracting (15) from (22) eliminates several terms. We can replace the advective term $\mathbf{u}' \cdot \nabla T'$ with $\boldsymbol{\nabla} \cdot (\mathbf{u}'T')$ due to (13). Taking the horizontal average of (22), this advective term can be reduced to

$$\frac{1}{4}\int_0^4 \boldsymbol{\nabla} \cdot (\mathbf{u}'T')dx = \frac{\partial}{\partial z}\langle w'T' \rangle \tag{23}$$

where $\langle \cdot \rangle$ denotes the horizontal average. The remaining terms in (22) are unaffected as they are independent of x. The eigenfunctions $W(z)$, $U(z)$, $\Theta(z)$, and $P(z)$ do not admit any natural normalization, as (13) - (15) and their subsequent forms are linear with respect to the perturbations. For completeness, we provide the normalization

$$\int_{-\frac{1}{2}}^{\frac{1}{2}} \big|\Theta(z)\big| dz = 1 \tag{24}$$

and assign each perturbation a yet-unknown amplitude $A \in \mathbb{R}$, thereby allowing us to rewrite (22) as an initial value problem (IVP)

$$\frac{\partial \bar{T}}{\partial t} + A^2 \langle w'T' \rangle = \mathcal{P}\frac{\partial^2 \bar{T}}{\partial z^2} \tag{25}$$

upon which the remainder of this investigation is centered. It is important to keep in mind that the forcing term $\langle w'T' \rangle$ is obtained by solving an eigenvalue problem (EVP) which itself involves $\frac{\partial \bar{T}}{\partial z}$. We assume that stable modes do not affect the evolution of $\bar{T}$.

For various Ra and fixed $Pr = 1$, we seek symmetric, marginally-stable temperature profiles $\bar{T}_{eq}(z)$ which are thermally equilibrated, thereby satisfying $\frac{\partial \bar{T}_{eq}}{\partial t} = 0$ according to (25). We employ the `Dedalus` pseudo-spectral python framework to solve the EVP outlined in Section II as well as the IVP (25) by representing each field with a dealiased Chebshev polynomial basis. The necessary number of basis functions varies, as temperature profiles associated with large Rayleigh numbers require increasingly small-scale structures to resolve their aggressive boundary layers. We supplement `Dedalus` with the `Eigentools` package to obtain the eigenfunctions in (25).

To find an equilibrated profile, we begin with a marginally-stable initial profile $\bar{T}_0(z)$ whose construction is outlined in III A. We seek to evolve $\bar{T}_0(z)$ into a new marginally-stable profile $\bar{T}_1(z)$ according to (25) using forward-Euler. This generally involves a unique and unknown value $A^2 > 0$. Our method of finding A^2 is best illustrated through example.

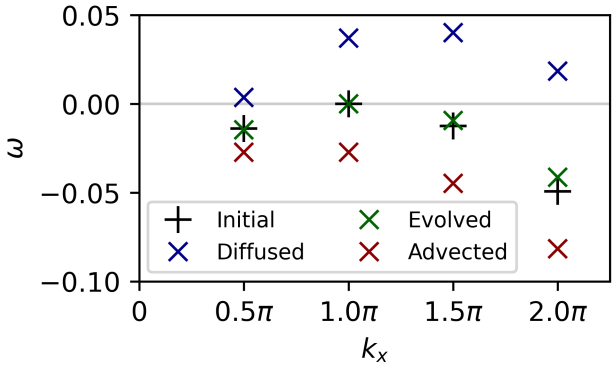

FIG. 1. Eigenvalue spectra for $Ra = 10^5$. The spectrum of a marginally-stable background temperature profile $\bar{T}_0$ (shown in black) has a maximum eigenvalue of 0. Given a small constant timestep Δt, diffusion destabilizes the system, increasing its eigenvalues (shown in blue). Advection tends to stabilize the system, decreasing its eigenvalues (shown in red). It follows that there exists some proportion (A^2) of these two terms which yields a new marginally-stable background temperature profile $\bar{T}_1$, whose spectrum is shown in green.

An iteration is performed as follows: diffusing a marginally-stable temperature profile $\bar{T}_0$ tends to increase its eigenvalues. Ignoring the diffusive term and evolving according to advection tends the stabilize the system. The appropriate amplitude A^2 can then be approximated by

$$A^2 \sim -\frac{\omega_{\text{diff}}}{\omega_{\text{adv}}} \tag{26}$$

where ω_{diff} and ω_{adv} refer to the diffused and advected eigenvalues (corresponding to the blue and red points respectively at $k_x = \pi$ in Figure 1) of the previously marginal mode. $\bar{T}_0$ is then evolved according to (25) and another eigenvalue solve is performed on the evolve temperature profile. Given a fixed timestep Δt, we assume the dominant eigenvalue can be described by a smooth function $\omega(A^2)$. Newton's method is used to find the appropriate amplitude by approximating $\omega'(A^2)$ with 1st-order finite-differences and specifying a tolerance $1e-9$. The dominant mode is not fixed; an iteration can facilitate the transfer of marginal-stability from one mode to another. In section III B we specify procedures for the treatment of multiple simultaneously marginal modes.

A. Initial buoyancy profile

In an attempt to minimize the required number of iterations, we employ the analytical thermal boundary layer equation for turbulent Rayleigh-Bénard convection given by **??**

$$\bar{T}_0(\xi) = \frac{\sqrt{3}}{4\pi}\log\frac{(1+a\xi)^3}{1+(a\xi)^3} + \frac{3}{2\pi}\arctan\left(\frac{4\pi}{9}\xi - \frac{1}{\sqrt{3}}\right) + \frac{1}{4}$$
$$\xi = \frac{z}{\delta_0}, \qquad a = \frac{2\pi}{3\sqrt{3}} \tag{27}$$

where δ_0 is the boundary layer thickness. We expect that each Ra is associated with a unique δ_0 for which $\bar{T}_0(z)$ is marginally-stable. It should be noted that when experimenting with different initial profiles, we obtain congruent equilibrated states, suggesting that these states may be unique. An example of (27) is given by the blue curve in Figure 2.

B. Treatment of multiple marginally-stable modes

In most cases, we eventually encounter eigenvalue spectra with multiple simultaneously marginal modes. If ignored, we are forced to reduce the timestep and allow the modes to alternate. Instead, we generalize the advective term in (25) to accommodate N simultaneously marginal modes

$$A^2\langle w'b'\rangle = \sum_{n=1}^{N} A_n^2\langle w'b'\rangle_n \tag{28}$$

where $\langle w'b'\rangle_n$ is composed of perturbations associated with $k_x = \frac{n\pi}{2}$. There are now N amplitudes to solve for and N eigenvalues to keep marginally-stable. In general, we expect a function $\omega : \mathbb{R}^N \to \mathbb{R}^N$ to have isolated roots (should they exist). We employ Broyden's method for root-finding in multi-dimensional functions whose derivatives are not explicitly known. Difficulty arises when transitioning between different numbers of marginal modes. Here we rely on $A^2 > 0$ by asserting that a mode which is *close enough* to marginal-stability can be included in the iteration provided that its respective amplitude is positive. Should we converge upon a negative amplitude, that mode is discarded and the iteration is repeated. In general we find that any other course of action fails to equilibrate.

IV. PROPERTIES OF THERMALLY EQUILIBRATED STATES

Thermally equilibrated states of this kind are solutions to the quasilinear Rayleigh-Bénard convection equations. For this investigation, we calculate solutions for Ra in the range $10^5 - 10^9$. Thermal equilibrium is synonymous with constant heat flux by (25). Solutions are symmetric about $z = 0$ by design. This, combined with the fact that we did initialize a background horizontal flow implies the absence of any nonconstant horizontal flow perturbations.

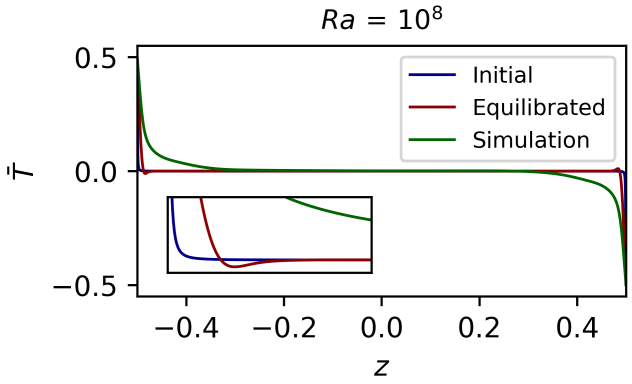

FIG. 2. Background temperature profiles $\bar{T}$ for $Ra = 10^8$. The initial profile is given by (27). The equilibrated curve refers to the background temperature profile of the marginally-stable thermally equilibrated state. The simulation profile is obtained by performing a 2-dimensional nonlinear simulation with `Dedalus` until thermal and kinetic relaxation. The simulation temperature data are horizontally and time averaged. The initial, equilibrated, and simulation profiles have increasingly relaxed boundary regions (respectively). The equilibrated profile exhibits prominent dips, nested alongside the boundary regions. The purpose of this feature is not well understood.

Figure 2 gives temperature profiles for $Ra = 10^8$, where the initial profile, given by (27), is employed at iteration 0; the equilibrated profile corresponds to the thermally relaxed state; and the simulation profile is obtained by performing a nonlinear simulation of (1)-(3) with `Dedalus`, followed by horizontal and time averaging. The simulation curve is more diffuse than the equilibrated curve, which in turn, is more diffuse than the initial curve. Performing an eigenvalue solve by setting $\bar{T}$ equal to the simulation profile yields positive eigenvalues. Comprehensively, this suggests that thermally-

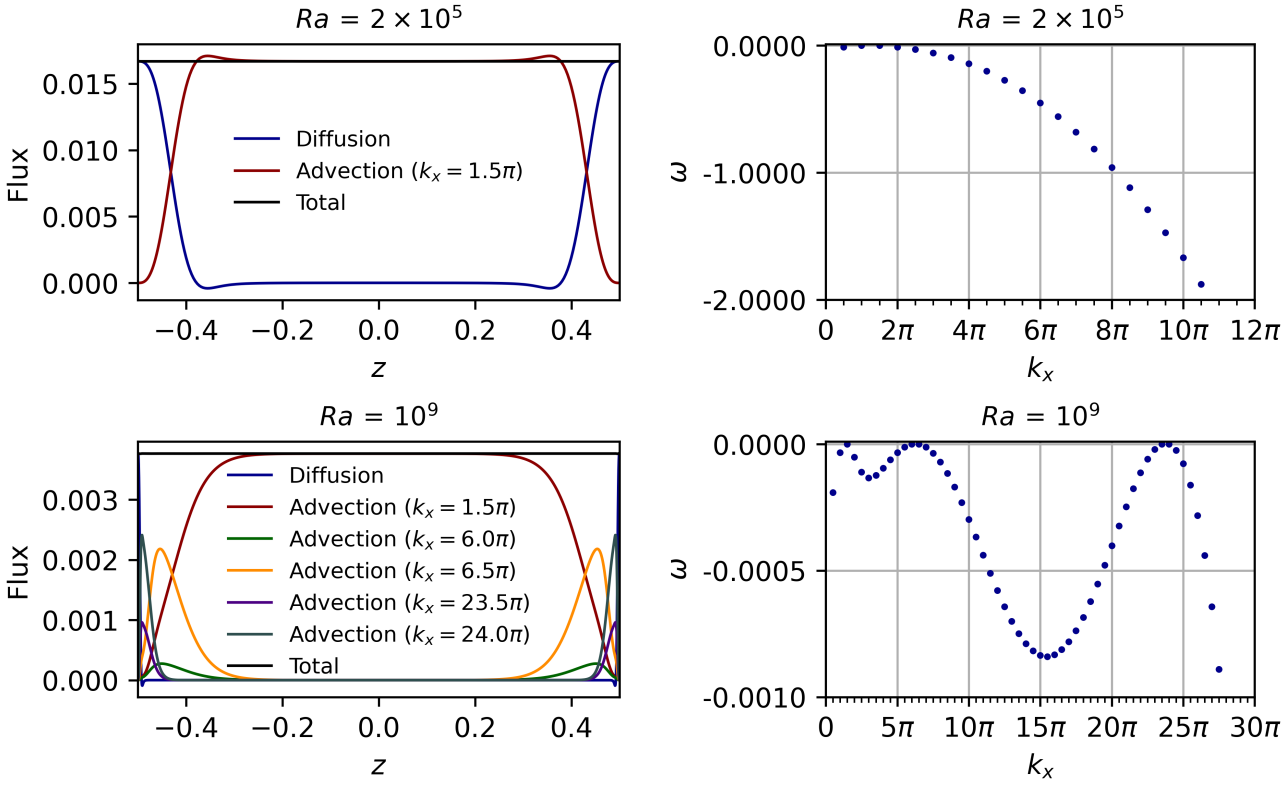

FIG. 3. Heat fluxes (left) and eigenvalue spectra (right) of equilibrated states $Ra = 2 \times 10^5$ (top) and $Ra = 10^9$ (bottom). Advection profiles belong to marginally-stable modes. For low Ra a single mode with $k_x = 1.5\pi$ is sufficient to oppose boundary layer diffusion and facilitate heat flux throughout the bulk of the domain. For large Ra, high-wavenumber marginally-stable modes contribute pronounced small-scale advection profiles which tightly hug the thin boundary layers. A combination of these of gradually widening advection profiles is necessary to transition to the $k_x = 1.5\pi$ mode.

equilibrated states might maximize boundary layer thickness, while subject to the marginal stability constraint.

The most resilient and unexpected feature of thermally equilibrated background temperature profiles are the pronounced dips adjacent to the boundary layers. These dips appear in every solution, regardless of Ra. Physically, they correspond to thin layers in which the temperature gradient reverses. This counter-diffusion, which opposes the overall heat transfer, is overcome by the coinciding advective flux, shown in Figure 3.

Equilibrated states exhibit distinct behaviors for large and small Ra. This contrast is illustrated in Figure 3, where we give heat flux profiles and eigenvalue spectra for two cases: $Ra = 2 \times 10^5$ and $Ra = 10^9$. For lower Ra, there is a single presumed local maximum in the eigenvalue spectrum, whose adjacent modes' advection profiles occupy the bulk of the domain. These states have relaxed boundary regions which gradually subside as the advection becomes the dominant component of the total flux. These transitional regions do not appear in high Ra cases, where the shift from diffusion to advection is sharp, requiring pronounced, small-scale advection profiles belonging to modes adjacent to the third presumed local maximum in the eigenvalue spectrum. Traversing towards the midplane of the domain, we see increasingly thicker advection profiles corresponding the wavenumbers adjacent to the second local maximum, eventually culminating in the dominant $k_x = 1.5\pi$ mode.

Thermally equilibrated states with large Ra tend to have a more diverse set of marginal modes as compared to small Ra state. In every case, the $k_x = 1.5\pi$ mode is included and is often unaccompanied by adjacent modes. In Figure 5 we give the wavenumbers k_x of marginal modes, color coded accordingly to their adjacency to each other. Marginal modes often appear in neighboring pairs, in which case the larger mode is denoted with an x marker and the smaller mode is denoted with a + marker. In these cases we infer the existence of a local maximum eigenvalue between the two adjacent marginally-stable modes. For $Ra \geq 10^6$, a second branch of marginal modes is introduced as shown in green, increasing according to some power-law with respect to Ra. The introduction of this largest branch is likely required to oppose the diffusion of the thinner boundary layers. For $Ra \geq 10^8$, a third branch of modes appears (shown in red), splitting the widening gap between the blue branch and the green branch. This development is associated with the relatively thick advection profiles, filling a niche

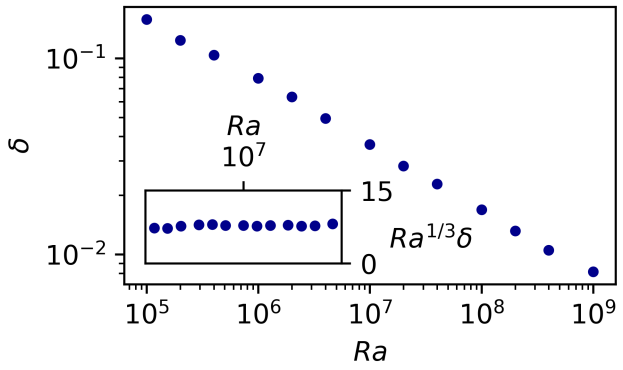

FIG. 4. Boundary layer widths δ of marginally-stable thermal equilibria. We define the threshold of each boundary layer as the z-coordinate at which $\frac{\partial \bar{T}}{\partial z} = 0$, corresponding to the local extrema of the equilibrated curve in Figure 2. Plotting on a log-log scale, we find δ and Ra obey a power-law relationship. We also demonstrate that $Ra^{1/3}\delta$ is approximately constant with respect to Ra implying $Ra \propto \delta^{-3}$, as predicted by **??** (scaling arguments literature)

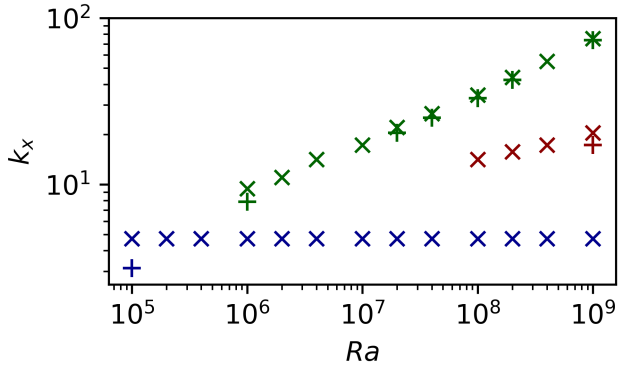

FIG. 5. Wavenumbers of marginally-stable modes of thermally equilibrated states. Markers are color-coded according to their adjacent local maxima index in the eigenvalue spectrum. For example, the spectrum corresponding to $Ra = 10^5$ has marginal wavenumbers $k_x = \pi$, 1.5π adjacent to a presumed local maximum between these two allowed values. The $Ra = 10^9$ spectrum, shown in lower right corner of Figure 3, has three presumed local maxima, with a single marginal mode adjacent to the first maximum ($k_x = 1.5\pi$), two marginal modes adjacent to the second maximum ($k_x = 6\pi$, 6.5π), and two marginal modes adjacent to the third maximum ($k_x = 23.5\pi$, 24π). The largest wavenumbers of the green branch obey a power-law relationship with Ra

in the total flux by uniting the sharp advection profiles of the largest branch (green) and the bulk-domain-oriented smallest branch (blue).

In general, marginally-stable thermal equilibria can be characterized by their boundary layer thicknesses, from which, the rest of their properties follow. Letting the interior boundary layer threshold be the z-coordinate at

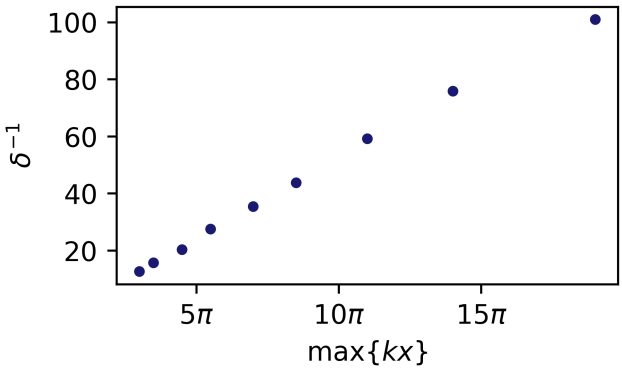

FIG. 6. For $Ra \geq 10^6$, the maximum marginally-stable wavenumber (corresponding to the green X markers in Figure 5) are inversely related to the boundary layer thicknesses δ. $(\max\{k_x\})^{-1}$ gives a minimum x length scale for the perturbations, and consequently, the advection. We expect the minimum z length scale to agree with the boundary layer thickness δ because otherwise the boundary layer would continue to diffuse. This is well illustrated in the lower left corner of Figure 3, where the advection profile for $k_x = 24\pi$ is tightly flanked by the surrounding boundary layers. This suggests that the minimum x and z length scales obey some constant ratio.

which $\frac{\partial \bar{T}}{\partial z} = 0$, we find that $Ra \propto \delta^{-3}$ as illustrated in Figure 4. This is consistent with Malkus' marginal-stability theory, a scaling argument which perceives the boundary regions as subdomains which are themselves marginally-stable **??**.

Nusselt numbers Nu for marginally-stable thermally-equilibrated states and direct numerical simulations are given in Figure 7. Marginally-stable Nu exceed simulation Nu, in agreement with the differing boundary layer geometries shown in Figure 2. Both datasets exhibit power-law relationships with Ra, and more specifically, $Ra \sim Nu^3$ which agrees with Figures 4, 5, and 6 and the scaling argument given by **??**.

V. SIMULATIONS WITH THERMALLY EQUILIBRATED INITIAL CONDITIONS

This is investigation is partially motivated by the prospect of decreasing nonlinear simulation relaxation times by employing thermally-equilibrated initial conditions. Conventionally, (1) - (3) are solved via direct numerical simulation (DNS) with initial conditions

$$T(x,z)\big|_{t=0} = 0.5 - z \tag{29}$$
$$\mathbf{u}(x,z)\big|_{t=0} = \mathbf{0} \tag{30}$$
$$p(x,z)\big|_{t=0} = 0 \tag{31}$$

which will hereby be referred to as the conductive initial condition. t in this section now refers to the simulation time as opposed to the thermal equilibration time

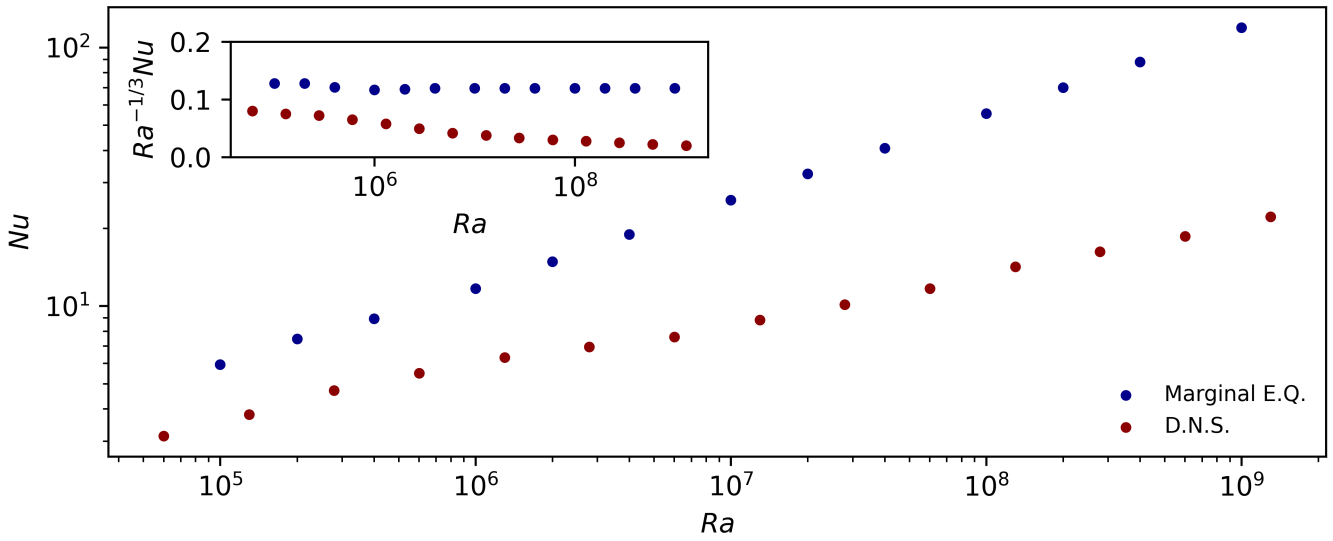

FIG. 7. Nusselt numbers are shown for marginally-stable thermally-equilibrated states and statistically-steady nonlinear simulations performed on Equations (1) - (3) with ??? other spectral methods ???. Both obey power-law relationships with Ra, with $Ra \sim Nu^3$ in agreement with Figures 4, 5, and 6 as well as **??** Malkus??? ($\gamma = 3$ marginally-stable boundary layer scaling argument). Marginally-stable states' Nusselt numbers exceed simulation Nusselt numbers. This can be well explained by the contrasting boundary region geometries shown in Figure 2.

parameter used previously. We define the equilibrated initial conditions

$$T(x,z)\big|_{t=0} = \bar{T}(z) + \sqrt{2}\sum_{n=1}^{N} A_n^2 \ \mathrm{Re}\Big[\Theta_n(z) e^{ik_{x_n}x}\Big]$$

$$\mathbf{u}(x,z)\big|_{t=0} = \sqrt{2}\sum_{n=1}^{N} A_n^2 \ \mathrm{Re}\Big[\Big(U_n(z)\hat{x} + W_n(z)\hat{z}\Big) e^{ik_{x_n}x}\Big]$$

$$p(x,z)\big|_{t=0} = \sqrt{2}\sum_{n=1}^{N} A_n^2 \ \mathrm{Re}\Big[P_n(z) e^{ik_{x_n}x}\Big] \qquad (32)$$

Where $\Theta_n(z), U_n(z), W_n(z), P_n(z)$; A^2; and k_{x_n} refer to the complex eigenfunctions, amplitude, and wavenumber at the nth marginal mode. The $\sqrt{2}$ factor is necessary normalize the eigenfunctions according to the new domain ???. By construction, these initial conditions are thermally equilibrated. Simulations launched with equilibrated initial conditions do not exhibit a convective-transient period, as the large-scale anatomy of the characteristic plumes and convective winds of Rayleigh-Bénard convection exist on initialization. This is illustrated in Figure 8, where the sharp spike in Nu is associated with the turbulent transition period of upwelling until the distinctive jet-like structure is established.

The marginally-stable equilibria are associated with a combination of eigenfunctions whose average kinetic energy is significantly larger than the statistical steady state, as given by Figure 9. This is impairs kinetic relaxation because the large horizontal flows decay on a viscous timescale

$$t_\nu \sim \frac{Pr}{\sqrt{Ra}}.$$

Consequently, marginally-stable thermally-equilibrated initial conditions do not reduce the simulation time required to achieve a statistically steady state, rather, they increase it considerably.

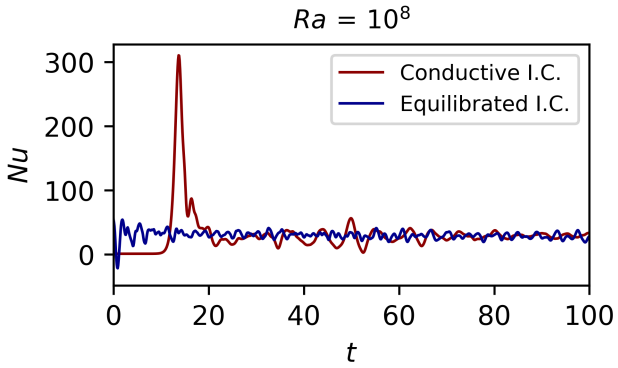

FIG. 8. Nusselt numbers of simulations performed at $Ra = 10^8$ with conventional initial conditions (red) and marginally-stable thermally-equilibrated initial conditions (blue). Simulations launched with thermally-equilibrated states do not undergo a convective-transient period because the characteristic plume structure exists on initialization. This is illustrated by the Nu spike at $t \sim 15$ in the convectional simulation.

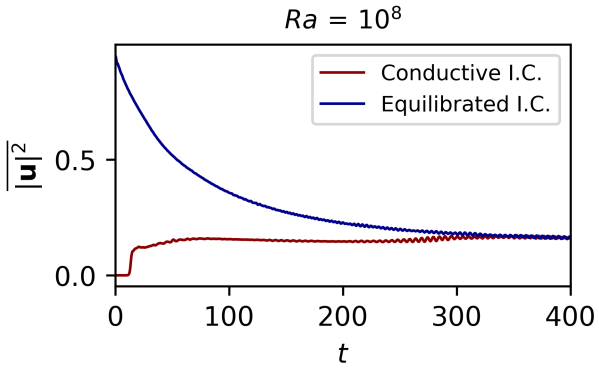

FIG. 9. Average kinetic energies of the same simulations performed in Figure 8 ($Ra = 10^8$). The combination of eigenfunctions which give thermal equilibrium have significantly more kinetic energy than the statistically steady state. Kinetic equilibrium is achieved according to the viscous timescale $t_\nu \sim PrRa^{-1/2}$.

VI. CONCLUSION

APPENDIX

This is an appendix

ACKNOWLEDGMENTS

We thank the people of Ohio.